Received: 5 May 2021 | Revised: 8 April 2022 | Accepted: 21 April 2022

DOI: 10.1002/glia.24186

GLIA

WILEY

RESEARCH ARTICLE

Cyclin-dependent kinase 7 contributes to myelin maintenance in the adult central nervous system and promotes myelin gene expression

Valérie Dion[1] | Nathalie Schumacher[1] | Nathalie Masar[1] | Alexandra Pieltain[1] | Pierre Tocquin[2] | Pierre Lesoinne[1] | Brigitte Malgrange[3] | Renaud Vandenbosch[3,4] | Rachelle Franzen[1]

[1]Laboratory of Nervous System Disorders and Therapies, GIGA Neurosciences, University of Liège, Liège, Belgium

[2]CARE PhytoSYSTEMS, Integrative Biological Sciences, University of Liège, Liège, Belgium

[3]Laboratory of Developmental Neurobiology, GIGA Stem Cells & GIGA Neurosciences, University of Liège, Liège, Belgium

[4]Division of Histology, Department of Biomedical and Preclinical Sciences, University of Liège, Liège, Belgium

Correspondence
Renaud Vandenbosch, Laboratory of Developmental Neurobiology, GIGA Stem Cells & GIGA Neurosciences, University of Liège, Liège, Belgium.
Email: rvandenbosch@uliege.be

Rachelle Franzen, Laboratory of Nervous System Disorders and Therapies, GIGA Neurosciences, University of Liège, Liège, Belgium.
Email: rfranzen@uliege.be

Funding information
Léon Fredericq Foundation, University of Liege; Fondation Charcot, Belgium; Fonds De La Recherche Scientifique - FNRS

Abstract

Mechanisms regulating oligodendrocyte differentiation, developmental myelination and myelin maintenance in adulthood are complex and still not completely described. Their understanding is crucial for the development of new protective or therapeutic strategies in demyelinating pathologies such as multiple sclerosis. In this perspective, we have investigated the role of Cyclin-dependent kinase 7 (Cdk7), a kinase involved in cell-cycle progression and transcription regulation, in the oligodendroglial lineage. We generated a conditional knock-out mouse model in which Cdk7 is invalidated in post-mitotic oligodendrocytes. At the end of developmental myelination, the number and diameter of myelinated axons, as well as the myelin structure, thickness and protein composition, were normal. However, in young adult and in aged mice, there was a higher number of small caliber myelinated axons associated with a decreased mean axonal diameter, myelin sheaths of large caliber axons were thinner, and the level of some major myelin-associated proteins was reduced. These defects were accompanied by the appearance of an abnormal clasping phenotype. We also used an in vitro oligodendroglial model and showed that Cdk7 pharmacological inhibition led to an altered myelination-associated morphological modification combined with a decreased expression of myelin-specific genes. Altogether, we identified novel functions for Cdk7 in CNS myelination.

KEYWORDS
central nervous system, cyclin-dependent kinase 7, myelin, myelination, oligodendrocyte precursor cell, post-mitotic oligodendrocyte

1 | INTRODUCTION

Myelin is a specialized lipidic membrane that wraps around axons and allows a rapid saltatory conduction through the concentration of voltage-dependent sodium channels at the nodes of Ranvier. It is generated by oligodendrocytes in the central nervous system (CNS) and by Schwann cells in the peripheral nervous system (PNS). Myelination is a complex process that can be summarized in four main steps in the CNS: (1) the proliferation and migration of oligodendrocyte precursor cells (OPCs), (2) the recognition of target axons, (3) the differentiation of OPCs into myelinating oligodendrocytes and (4) axonal wrapping, myelin formation and compaction (Bauer et al., 2009; Simons & Nave, 2015; Stadelmann et al., 2019). All of these steps are

Valérie Dion and Nathalie Schumacher contributed equally as first authors.

Renaud Vandenbosch and Rachelle Franzen contributed equally as last authors.

highly regulated and only some of the regulating mechanisms have been discovered so far (for reviews, see Emery, 2010; Emery & Lu, 2015).

Due to myelin major role in CNS physiology, myelin defects have important deleterious consequences and lead to invalidating diseases. The most frequent human demyelinating disease is multiple sclerosis (MS) which is characterized by myelin degradation with the formation of multifocal lesions (called plaques) and a progressive axonal demyelination, leading to the clinical disability observed in patients (Compston & Coles, 2008). Even if evidence of remyelination have been found in demyelinated lesions, myelin repair ultimately fails or remains incomplete (Stadelmann et al., 2019).

A better understanding of the mechanisms involved in oligodendrocyte differentiation, myelin formation and remyelination is crucial to help identify new targets for the development of therapies. Indeed, enhancement of endogenous remyelination has lately emerged as a promising therapeutic approach in MS (Cunniffe & Coles, 2019).

Cyclin-dependent kinases (Cdks) are serine–threonine kinases whose activity depends on their association with specific regulatory proteins called cyclins. In metazoans, Cdks are divided into two groups: the cell-cycle Cdks, and those implicated in transcription regulation (Malumbres & Barbacid, 2005). Cyclin-dependent kinase 7 (Cdk7) is a special member of this family, as it is involved in both processes. It associates with cyclin H and Mat1 to form the Cdk-activating kinase (CAK) complex which phosphorylates and activates cell-cycle Cdks. The CAK complex, along with the helicases XPD and XPB and the subunits p62, p52, p44, p34, and p8, constitute the general transcription factor TFIIH which is involved in transcription regulation through the phosphorylation of serine residues located in the C-terminal domain (CTD) of RNA Polymerase II (RNA Pol II) (Compe & Egly, 2012; Fisher, 2005). In addition, Cdk7 phosphorylates and regulates the activity of several nuclear receptors including retinoic acid receptor α (RARα), estrogen receptor α (ERα) and peroxisome-proliferator-activated receptors (PPARs) (Chen et al., 2000; Compe et al., 2005; Rochette-Egly et al., 1997).

This last decade, Cdk7 has emerged as an interesting therapeutic target in numerous types of cancers thanks to the development of covalent inhibitors. For example, THZ1 has been shown to inhibit tumor growth through its action on the transcriptional machinery (for reviews, see Li et al., 2019; Wang et al., 2020). In mouse, genetic ablation of Cdk7 leads to cell division arrest and early embryonic lethality, showing its critical importance during cell cycle progression and development. However, Cdk7 seems dispensable for global transcription, as RNA Pol II mediated transcription is mostly unaffected (Ganuza et al., 2012). It seems indeed that Cdk7 is rather involved in specific transcriptional programs. In support of this hypothesis, the genetic ablation of Mat1—the assembly factor of the CAK complex—in Schwann cells leads first to a normal myelination of the sciatic nerve, followed by a progressive demyelination starting after 3 months of age (Korsisaari et al., 2002). In the CNS, Cdk7 has been shown to be important for the regulation of transcription-dependent neuronal functions such as activity-induced neuronal gene expression, synaptic plasticity and the formation of long-term memories (He et al., 2017). In addition, mutations of the helicase XPD—the subunit which bridges the CAK complex to the core of TFIIH—result in hypomyelination in the CNS of both human and mice (Compe et al., 2007).

In this study, we hypothesize that Cdk7 regulates the transcription of genes involved in CNS myelination. We show that genetic invalidation of Cdk7 in oligodendrocytes allows normal developmental myelination but progressively leads to myelin defects and hindlimb clasping phenotype in young adult and aged mice. Moreover, pharmacological inhibition of Cdk7 in vitro impairs myelination-induced morphological changes and reduces oligodendroglial gene expression. Altogether, we demonstrate here an important role for Cdk7 in CNS myelination.

2 | MATERIALS AND METHODS

2.1 | Mice

To specifically knock-out Cdk7 in post-mitotic oligodendrocytes, mice with Cdk7 floxed genes (Ganuza et al., 2012) were crossed with mice expressing the Cre-recombinase gene under the control of the Cnp1 regulatory sequence (Lappe-Siefke et al., 2003). Genotypes of all mice were determined using a PCR analysis of tail genomic DNA with appropriate primers (Table S1). Mice were kept on a mixed C57BL/6-SV129 genetic background. Male and female were used in the same ratio. Mice were housed in a controlled environment with free access to food and water, on a 12 h light/dark cycle. All experiments were performed in accordance with the Animal Ethics Committee of the University of Liège.

2.2 | RNAscope

RNAscope was performed using the RNAscope Multiplex Fluorescent V2 Assay (ACD). Briefly, mice were perfused with 4% PFA and lumbar spinal cord and brain were dissected. Tissues were post-fixed in 4% PFA for 24 h at 4°C, cryopreserved in increasing concentration of sucrose (10, 20 and 30%), and then frozen in OCT embedding medium. Ten micrometre thick sections were cut in a cryostat and mounted on Superfrost Plus slides, with a single section per slide. The rest of the assay was performed according to the manufacturer's protocol. Probes used were RNAscope Probe Mm-Cnp (ACD #472241) and RNAscope Probe Mm-Cdk7-C2 (ACD #573911-C2), Opal dyes used were Opal 650 and Opal 570 Reagent Packs (Akoya Biosciences FP1496001KT and FP1488001KT). Images were obtained with a Nikon A1R confocal microscope, and analyzed with ImageJ at the ventral funiculi level for spinal cord sections and at the corpus callosum level for brain sections. Three representative fields were analyzed for each animal.

2.3 | Toluidine blue staining and transmission electron microscopy

Mice were perfused with 0.9% NaCl followed by 4% PFA. Lumbar spinal cord was dissected and post-fixed for 2 h in 0.1 M cacodylate

buffer pH 7.2 containing 2.5% glutaraldehyde at 4°C. An additional fixation step was carried out for 30 min in PO_4 buffer containing 1% osmium at 4°C. Samples were then dehydrated in graded ethanol baths, and finally embedded in epon resin. Semi-thin (1 μm) and ultra-thin (90 nm) sections were cut with a microtome. Semi-thin sections were collected on glass slides and stained with 0.5% toluidine blue. Ultra-thin sections were collected on Formvar/Carbon coated nickel grids and further contrasted with 5% uranyl acetate then lead citrate. Images were obtained using an Olympus AX-70 microscope for toluidine blue images, and either a Zeiss EM 910 or a Jeol JEM-1400 transmission electron microscope at 60 kV or 80 kV, respectively, for electron microscopy images, all at the ventral funiculi level, and were analyzed with ImageJ. The number of myelinated axons with their respective axonal diameter were quantified on toluidine blue images. Two representative fields were analyzed for each animal, with a mean of ∼3500 axons per animal. *g*-ratio were quantified on transmission electron micrographs. *g*-ratio was obtained by dividing the mean axonal diameter without myelin by the same axonal diameter with myelin. A mean of ∼250 axons per animal were analyzed, on at least five representative fields for each animal.

2.4 | Western blotting

Mice were perfused with 0.9% NaCl, lumbar spinal cord was dissected and then lysed with RIPA buffer (10 mM Tris–HCl pH 7.5, 150 mM NaCl, 1 mM EDTA, 1% NP-40, 0.1% sodium deoxycholate, 0.1% SDS, 10 mM NaF, 1 mM Na3VO4, complete protease inhibitor cocktail). Protein concentration was determined using Pierce BCA Protein Assay Kit (ThermoScientific). Fifteen or 10 μg of proteins—from P28 or 1-year spinal cords, respectively—were separated by SDS-PAGE and transferred onto PVDF membranes (GE Healthcare). Membranes were blocked for 1 h at room temperature (RT) with TBS containing 0.1% Tween 20 and 5% non-fat milk, incubated overnight at 4°C with the primary antibodies anti-MAG (Millipore MAB1567, 1:500), anti-CNP (Abcam ab227218, 1:1000), anti-MBP (Millipore MAB386, 1:500) and anti-PLP (Millipore MAB388, 1:1000), and for 1 hour at RT with the corresponding HRP-conjugated secondary antibodies (GE Healthcare). Incubation with HRP-conjugated anti-β-actin (Sigma A3854, 1:10.000) or anti-vinculin (Santa Cruz sc-73,614-HRP, 1:1000) antibodies was performed as loading control. Membranes were developed using ECL reagent (GE Healthcare). Protein relative expression was quantified with ImageJ.

2.5 | Hindlimb clasping test

Hindlimb clasping is an abnormal behavior exhibited when a mouse is held by the tail. To evaluate the presence of clasping, mice were suspended by the base of the tail for 15 s and the posture of the hindlimbs was observed. The response was considered as a clasping behavior when one or both hindlimbs were retracted and touched the abdomen for more than 3 s during the suspension, whereas an absence of clasping consisted of both hindlimb being abducted away from the abdomen. Three trials were performed in each session of observation, and mice were observed every 2 weeks from 8-weeks-old to 52-weeks-old. For analysis, only mice which exhibited a clasping behavior over two consecutive sessions of observation and maintained this behavior over time were considered as having a clasping behavior.

2.6 | Cell culture

Oli-neu cells were used as originally described (Jung et al., 1995). The cells were cultured at 37°C with 5% CO_2, on surfaces coated with poly-L-lysine. They were expanded in Sato medium supplemented with 2% horse serum (DMEM with 0.2% [w/v] sodium bicarbonate, 100 μM putrescine, 10 μg/ml transferrin, 10 μg/ml insulin, 520 nM thyroxine, 500 nM triiodothyronine, 200 nM progesterone and 220 nM sodium selenite). Differentiation was induced by adding 1 mM dibutyryl-cAMP (referred as cAMP) to the medium for 1 or 3 days. Pharmacological inhibition of Cdk7 was induced by adding 250 nM YKL-5-124 (Olson et al., 2019) to the medium for 1 or 3 days. The same concentration of 0.1% DMSO was used in all conditions, and medium containing 0.1% of DMSO was used as vehicle.

2.7 | Immunocytochemistry

For immunocytochemistry, Oli-neu cells were fixed in 4% paraformaldehyde (PFA) for 10 min at RT. Blocking was performed for 1 h at RT in PBS containing 0.3% Triton X-100 and 10% normal donkey serum. The cells were incubated overnight at 4°C with the primary antibody anti-O4 (Millipore MAB345, 1:500) and then for 1 h at RT with the secondary antibody coupled to FITC (Jackson ImmunoResearch). DAPI was applied to stain the nuclei. Images were obtained with an Olympus AX-70 microscope and were submitted to the Sholl analysis.

2.8 | Sholl analysis

Morphology of the O4-labeled processes branching out of the cell bodies of Oli-neu cells was assessed using Sholl analysis. Images containing isolated cells were selected and converted to 8-bit, and cell projections were manually traced. Traced projections were then analyzed using the Sholl analysis plug-in of ImageJ. From the center of the cell, concentric circles with an increasing diameter were placed and the number of intersections with each circle was counted. This analysis was performed for 100 cells per condition, in three independent experiments.

2.9 | RNA extraction, cDNA synthesis and real-time quantitative PCR (RT-qPCR)

RNA was extracted using RNeasy Mini Kit (Qiagen) and contaminating DNA was degraded using RNase-Free DNase Set (Qiagen),

both according to the manufacturer's protocol. cDNA was synthesized from RNA using RevertAid First Strand cDNA Synthesis Kit (ThermoScientific). RT-qPCR was then performed using GoTaq qPCR Master Mix (Promega). A melting curve was obtained for each PCR product in each run to control gene-specific peaks. β-actin, Gapdh and Hprt were run as housekeeping genes. Relative expression was calculated using the $2^{-\Delta\Delta CT}$ method for each housekeeping gene independently. Data shown in graphs are relative expression to β-actin. PCR primers sequences are listed in Table S2.

2.10 | Statistical analysis

Each in vitro experiment was repeated independently three times. The number of animals used for each in vivo experiment is specified in the figure legends. Data are expressed as mean ± standard error of the mean (SEM) in connecting line graphs and bar graphs, and as median with 10–90 percentile in box&whiskers graphs. Statistical analysis was done using GraphPad Prism 7. Tests used are specified in the figure legends. Significance was classified as follows: *: $p < .05$; **: $p < .01$; ***: $p < .001$; ****: $p < .0001$.

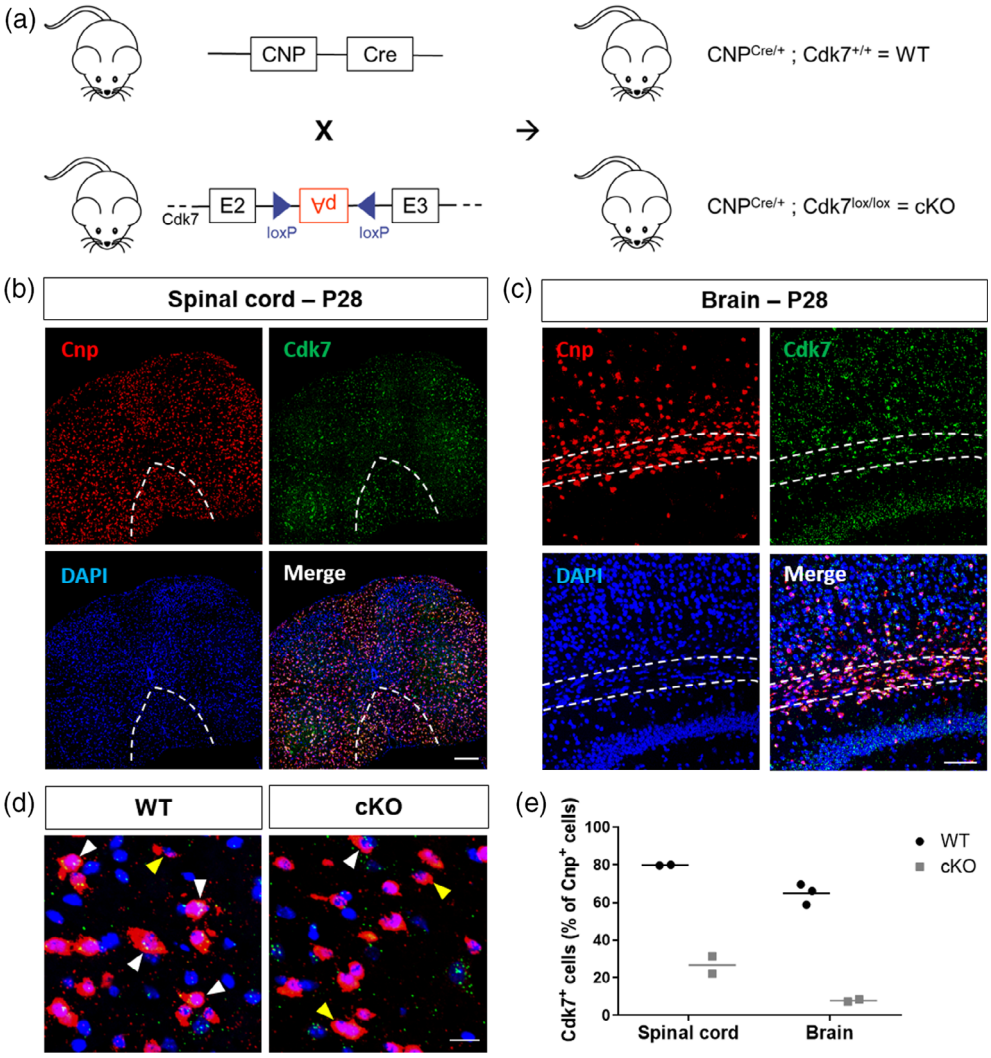

FIGURE 1 Cyclin-dependent kinase 7 (Cdk7) is invalidated in post-mitotic oligodendrocytes in CNP-Cdk7 KO mice. (a) Schematic representation of the generation of CNP-Cdk7 KO mice. $CNP^{Cre/+}$; $Cdk7^{lox/lox}$ (cKO) mice and their $CNP^{Cre/+}$; $Cdk7^{+/+}$ control littermates (WT) were obtained by crossing $CNP^{Cre/+}$; $Cdk7^{lox/+}$ mice with $CNP^{+/+}$; $Cdk7^{lox/+}$ mice. In the CNP-Cre mice, the Cre recombinase gene is under the control of the Cnp1 regulatory sequence. In the $Cdk7^{lox}$ allele, a cassette with a polyadenylation (pA) site in the inactive orientation surrounded by two loxP sites in opposite orientation has been inserted between exons 2 (E2) and 3 (E3). Cre-mediated recombination inverts the cassette to the active orientation and induces a premature termination of Cdk7 transcript. (b, c) Representative images of RNAscope assay in WT mice at P28 in (b) the spinal cord and (c) the brain. Cnp is labeled in red, Cdk7 in green. Nuclei are stained with DAPI. White dotted lines delimit the ventral funiculi in the spinal cord, and the corpus callosum in the brain. Scalebar = 200 μm in (b); 100 μm in (c). (d) Merge images at a higher magnification, in the spinal cord of WT and cKO mice. White arrowheads show $Cnp^+/Cdk7^+$ cells, yellow arrowheads show $Cnp^+/Cdk7^-$ cells. Scalebar = 20 μm. (e) Quantification of the percentage of $Cnp^+/Cdk7^+$ cells among all Cnp^+ cells, at the level of the ventral funiculi in the spinal cord and of the corpus callosum in the brain, in P28 WT and cKO mice ($n = 2–3$ for all groups).

3 | SUPPLEMENTARY MATERIALS AND METHODS

3.1 | Immunohistochemistry

For immunohistochemistry, mice were perfused with 0.9% NaCl followed by 4% PFA. Lumbar spinal cord was dissected and post-fixed overnight in 4% PFA at 4°C. The tissues were then cryopreserved in 30% sucrose and frozen in OCT embedding medium. Spinal cords were cut in a cryostat and mounted on Superfrost Plus slides (10 μm thick, transverse sections). Immunofluorescence was performed as described in the immunocytochemistry section, with the primary antibodies anti-Olig2 (Millipore AB9610, 1:500), anti-PDGF-Rα (R&D Systems AF1062, 1:500) and anti-APC (CC1, Calbiochem OP80, 1:250), and the corresponding secondary antibodies coupled to Alexa Fluor 488, Alexa Fluor 594 or Alexa Fluor 647 (Jackson ImmunoResearch). Images were obtained with a Nikon A1R confocal microscope, and analyzed with ImageJ at the ventral funiculi level. At least three representative fields were analyzed for each animal.

3.2 | Western blotting

Western blotting was performed as described before, with the following modifications: 50 μg of proteins were separated by SDS-PAGE, and the primary antibody used was anti-βAPP (Invitrogen 51-2700, 1:1000).

4 | RESULTS

4.1 | Genetic invalidation of Cdk7 in oligodendrocytes progressively leads to an increased number of small caliber myelinated axons

Cdk7 is known to be involved in transcription regulation, and has been shown to regulate specific transcriptional programs in the CNS. In order to investigate its specific role in CNS myelination, and since Cdk7 germline knock-out (KO) are embryonically lethal (Ganuza et al., 2012), we generated a conditional KO (cKO) model in which Cdk7 is invalidated in differentiating post-mitotic oligodendrocytes. Mice homozygous for the Cdk7 floxed gene ($Cdk7^{lox/lox}$) (Ganuza et al., 2012) were interbred with $CNP^{Cre/+}$ mice (Lappe-Siefke et al., 2003) to obtain $CNP^{Cre/+}$; $Cdk7^{lox/+}$ mice. These were then crossed with $CNP^{+/+}$; $Cdk7^{lox/+}$ mice to obtain $CNP^{Cre/+}$; $Cdk7^{lox/lox}$ mice (CNP-Cdk7 KO mice, referred as cKO) and their $CNP^{Cre/+}$; $Cdk7^{+/+}$ control littermates (referred as WT) (Figure 1a). This last crossing produced offspring at expected Mendelian ratios. cKO mice had a normal life expectancy and fertility, and their gross anatomy and weight were not altered.

To confirm whether Cdk7 was invalidated in oligodendrocytes, we performed a RNAscope assay using probes directed against Cnp and Cdk7. In WT mice, we observed that Cdk7 mRNA was widely expressed in oligodendrocytes at postnatal day 28 (P28). Indeed, Cdk7 mRNA expression could be detected in areas enriched in oligodendrocytes such as the ventral funiculi of the spinal cord (Figure 1b) and the corpus callosum in the brain (Figure 1c). As expected, Cdk7 mRNA expression in oligodendrocytes was reduced in cKO mice (Figure 1d), and the percentage of $Cnp^{+}/Cdk7^{+}$ cells among total Cnp^{+} cells was strongly decreased in cKO spinal cord and brain compared to WT (spinal cord: WT 79.84 ± 0.17% vs cKO 26.79 ± 4.66%—brain: WT 64.88 ± 3.18% vs cKO 7.92 ± 0.50%) (Figure 1e), thereby validating our model.

Using this CNP-Cdk7 KO mouse model, we investigated if CNS myelination was perturbed in the absence of Cdk7. Our investigations were performed at three selected ages: P28—a stage corresponding to the end of the developmental myelination in the CNS, 8–10 weeks—early adulthood in mice, and 1 year—allowing us to study the long-term consequences of Cdk7 invalidation in oligodendrocytes.

First, we evaluated the impact of Cdk7 invalidation on the number of myelinated axons in the spinal cord ventral funiculi by analyzing semi-thin sections stained with toluidine blue. No gross differences could be observed between WT and cKO mice, but the number of myelinated axons seemed higher in cKO mice compared to WT (Figure 2a). Quantification of the number of myelinated axons per surface unit confirmed our observations. Even though the number of myelinated axons was decreased over time in both WT and cKO mice, it remained higher in cKO mice compared to WT, and this difference became statistically significant at 8–10 weeks and 1 year (Figure 2b). In support of these results, we quantified the number of cells of the oligodendroglial lineage ($Olig2^{+}$ cells for all stages, PDGF-$R\alpha^{+}$ cells for OPCs, and $CC1^{+}$ cells for post-mitotic oligodendrocytes) and we observed that the number of oligodendroglial cells was significantly increased in cKO mice compared to WT at 8–10 weeks and 1 year, due to an increased number of post-mitotic oligodendrocytes (Figure S1).

We then focused on the axonal diameter of myelinated axons. Interestingly, the increase in the number of myelinated axons observed in cKO mice was associated with a significant reduction of the mean axonal diameter at all ages (Figure 2c). In order to gain more information about the smaller mean axonal diameter, we categorized myelinated axons depending on their axonal diameter (<1, 1–2, 2–3, and >3 μm). No significant differences were observed between WT and cKO mice in all categories of axons at P28 (Figure 2d), whereas the smallest caliber axons (<1 μm) were significantly increased in cKO mice at 8–10 weeks (Figure 2e), and both the number of <1 and 1–2 μm axons were significantly increased in cKO mice at 1 year (Figure 2f). In addition, even if the number of large caliber myelinated axons (>3 μm) was not significantly affected, their proportion (percentage of all myelinated axons) was reduced in cKO mice (Figure 2g). These results indicate that Cdk7 loss progressively leads to an increased number of small caliber myelinated axons associated with a reduction of the mean axonal diameter, and a reduced proportion of large caliber axons.

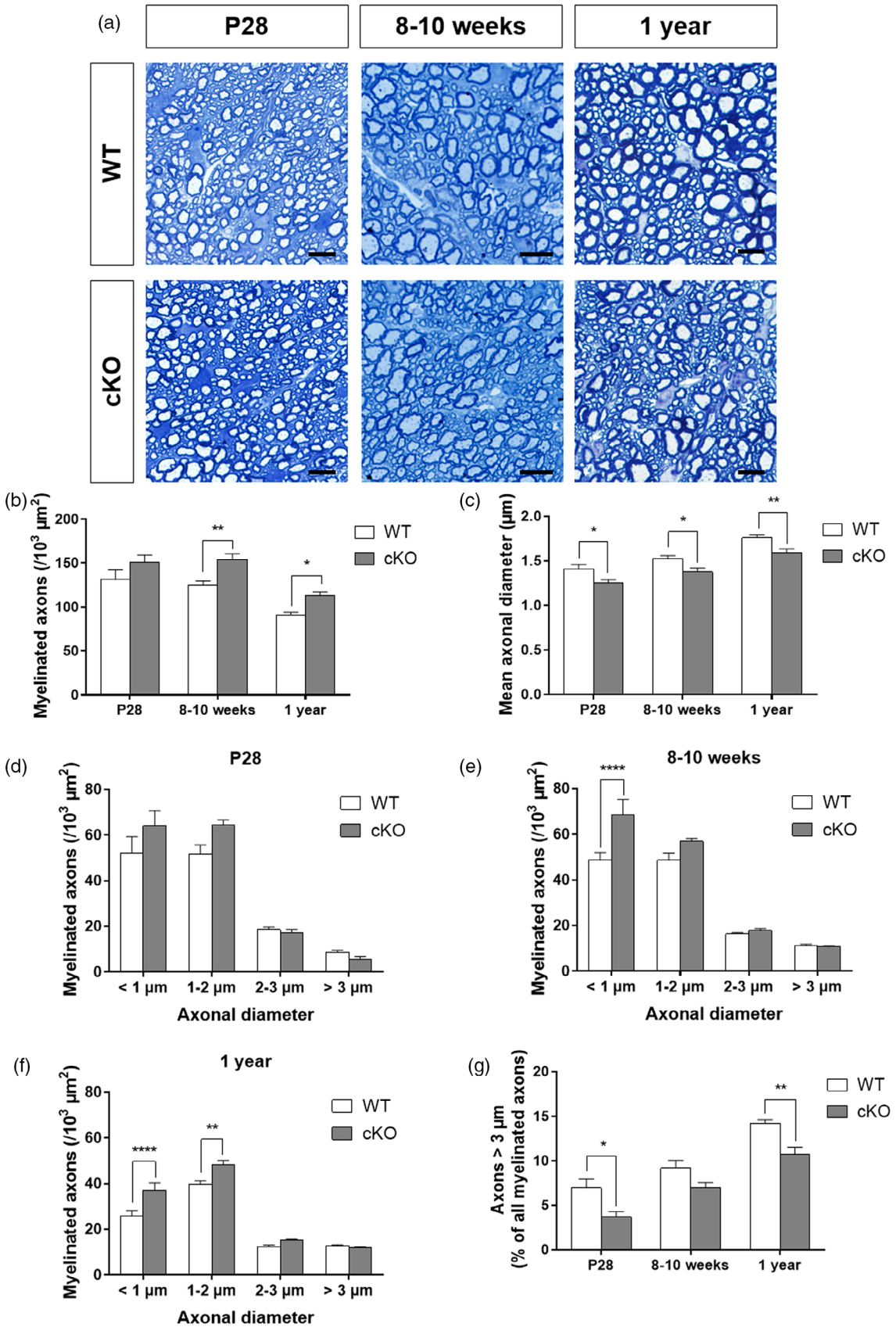

FIGURE 2 Legend on next page.

4.2 | Cdk7 invalidation progressively leads to myelin thinning in large caliber axons

The above results suggest that Cdk7 plays an important role in myelination, and that its role becomes more important when the mice get older, as abnormalities appear and progress with time. To validate this hypothesis, we analyzed the fine structure of the myelin sheath in the spinal cord at all ages by transmission electron microscopy. While normal myelin sheath structure could be observed and no gross morphological differences were detected between WT and cKO mice at P28, myelin sheath thickness seemed to be reduced in cKO mice at 8–10 weeks and 1 year (Figure 3a). We thus quantified myelin sheath thickness by measuring the *g*-ratio of myelinated axons. At P28, the median *g*-ratio was similar between WT and cKO mice (WT: 0.70—cKO: 0.71) (Figure 3b), and the distribution of *g*-ratios in relation with axonal diameter was comparable (Figure 3e). At 8–10 weeks, the median *g*-ratio was still similar (WT: 0.72—cKO: 0.73) (Figure 3c), but the distribution of *g*-ratios of cKO mice began to move away from the WT as the axonal diameter increased (Figure 3f). At 1 year, the median *g*-ratio was slightly increased in cKO mice compared to WT (WT: 0.69—cKO: 0.72) (Figure 3d), and the gap between the two distributions grew even bigger, especially as the axonal diameter increased (Figure 3g). As these results indicate that the myelin sheath becomes thinner mostly in large caliber axons, we calculated the mean *g*-ratio of axons separated into two categories depending on their axonal diameter: under and over 3 μm. While no differences could be observed between WT and cKO mice for the first category (Figure 3h), the mean *g*-ratio was significantly increased in cKO mice at 8–10 weeks and 1 year for the second category (Figure 3i). These results indicate that the myelin sheath of large caliber axons progressively becomes thinner in cKO mice compared to WT.

4.3 | Myelin protein content is modified in aged mice

Cdk7 invalidation progressively alters some aspects of myelination in young adult and in aged mice. In order to investigate if these defects were associated with a reduced myelin protein content, we quantified the amount of some of the most important CNS myelin proteins in the spinal cord: myelin-associated glycoprotein (MAG), 2′,3′-Cyclic-nucleotide 3′-phosphodiesterase (CNP), myelin basic protein (MBP) and proteolipid protein (PLP). At P28—when no major myelination defects could be observed yet—the amount of these proteins appeared similar between WT and cKO mice (Figure 4a,b), which was confirmed by quantification (Figure 4c–f). However, at 1 year—when the myelination defects observed were the most important—a decreased amount of those proteins could be observed in cKO mice (Figure 4g,h), with a statistically significant decrease for MAG and PLP (Figure 4i–l). These results indicate that Cdk7 invalidation also leads to an altered myelin protein content in aged mice.

4.4 | Myelin defects appear with age and lead to hindlimb clasping phenotype

As the animals were getting older, we noticed that cKO mice started to exhibit an abnormal behavior of hindlimb clasping when held by the tail (Figure 5a). This phenotype is a common manifestation of various brain and spinal cord pathologies (Lalonde & Strazielle, 2011). We started to observe this phenotype in 10-weeks-old mice in both genotypes, with a much higher percentage in cKO mice, which was increasing over time. Overall, the percentage of mice exhibiting this behavior was significantly higher in cKO mice compared to WT (Figure 5b). The appearance of the hindlimb clasping phenotype and its worsening over time in cKO mice indicate that the myelination defects observed in cKO mice could lead to functional consequences.

This hindlimb clasping phenotype did not appear to originate from axonal defects. Indeed, axonal damage was not increased in 1-year-old cKO mice, as evidenced by βAPP western blotting (Figure S2). Moreover, quantification of myelinated axons with axonal diameter over 3 μm in WT and cKO 1-year-old mice revealed no shrinkage of the axonal diameter over time. Even though the proportion of some categories of large caliber axons was decreased in cKO mice compared to WT (Figure S3b), this was not attributable to a difference in the number of these large caliber axons (Figure S3a), but rather to the overall increased number of all myelinated axons described in Figure 2.

4.5 | Pharmacological inhibition of Cdk7 alters myelination-associated changes in morphology and in transcription of myelin-specific genes

Our cKO mouse model allowed us to uncover myelination defects starting in young adults and getting worse in aged mice. In order to

FIGURE 2 Cyclin-dependent kinase 7 (Cdk7) invalidation progressively leads to an increased number of small caliber myelinated axons. (a) Representative images of toluidine blue staining in the ventral funiculi of lumbar spinal cord of WT and cKO mice at P28, 8–10 weeks and 1 year. Scalebar = 10 μm. (b) Quantification of the number of myelinated axons in WT and cKO mice at P28, 8–10 weeks and 1 year. (c) Quantification of the mean axonal diameter in WT and cKO mice at P28, 8–10 weeks and 1 year. (d to f) Quantification of the number of myelinated axons of <1, 1–2, 2–3, and >3 μm axonal diameter, in WT and cKO mice at (d) P28, (e) 8–10 weeks and (f) 1 year. (g) Quantification of the percentage of myelinated axons with axonal diameter over 3 μm among all myelinated axons, in WT and cKO mice at P28, 8–10 weeks and 1 year. All quantifications were performed in the ventral funiculi of lumbar spinal cords ($n = 6$ for P28 WT/cKO; $n = 7$ for 8–10 weeks WT/cKO; $n = 8$ for 1-year WT/cKO, *: $p < .05$; **: $p < .01$; ****: $p < .0001$, Two-way ANOVA—Sidak's multiple comparisons).

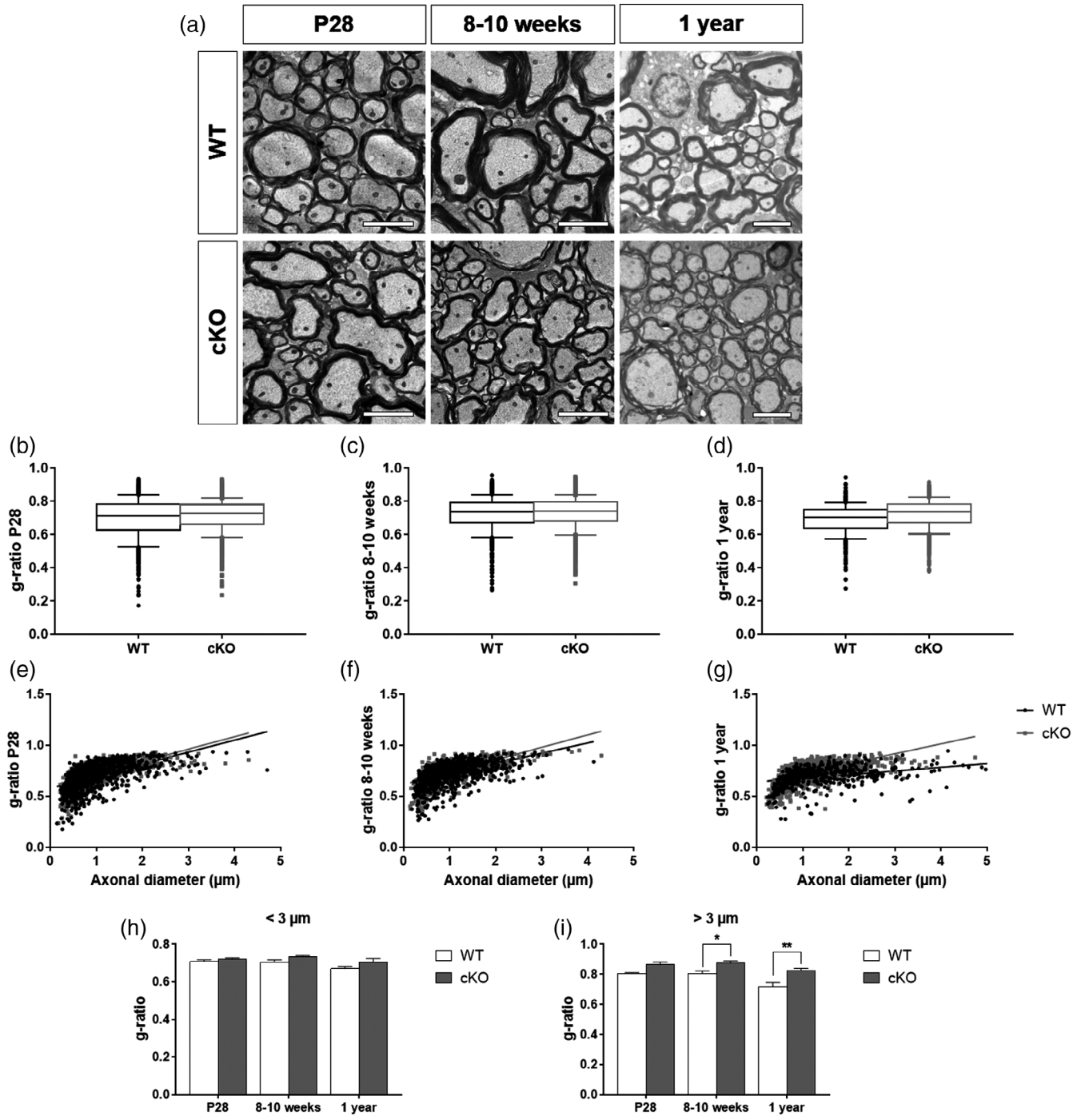

FIGURE 3 Cyclin-dependent kinase 7 (Cdk7) invalidation progressively leads to a thinner myelin sheath in large caliber axons. (a) Transmission electron micrographs of the ventral funiculi of lumbar spinal cord of WT and cKO mice at P28, 8–10 weeks and 1 year. Scalebar = 3 μm. (b–d) Quantification of the median *g*-ratio of myelinated axons in WT and cKO mice at (b) P28, (c) 8–10 weeks and (d) 1 year. (e–g) Relationship between *g*-ratio and axonal diameter in WT and cKO mice at (e) P28, (f) 8–10 weeks and (g) 1 year. (h, i) Quantification of the mean *g*-ratio of myelinated axons with an axonal diameter (h) under 3 μm and (i) over 3 μm in WT and cKO mice at P28, 8–10 weeks and 1 year. All quantifications were performed in the ventral funiculi of lumbar spinal cords ($n = 4–5$ for all groups in (a) and (h, i), 1058/1104 axons for P28 WT/cKO; 986/1201 axons for 8–10 weeks WT/cKO; 547/1782 axons for 1-year WT/cKO in (b–g), *: $p < .05$; **: $p < .01$, Two-way ANOVA—Sidak's multiple comparisons).

decipher the mechanisms underlying this phenotype in vitro, we treated Oli-neu cells—a well-known model of murine oligodendroglial cell culture in which a cAMP treatment induces changes that can be linked to early myelination (Jung et al., 1995)—with the recently developed YKL-5-124, a selective covalent inhibitor of Cdk7 (Olson et al., 2019).

We first assessed if the morphology of cAMP-treated Oli-neu cells was affected by YKL-5-124 treatment. To do so we performed

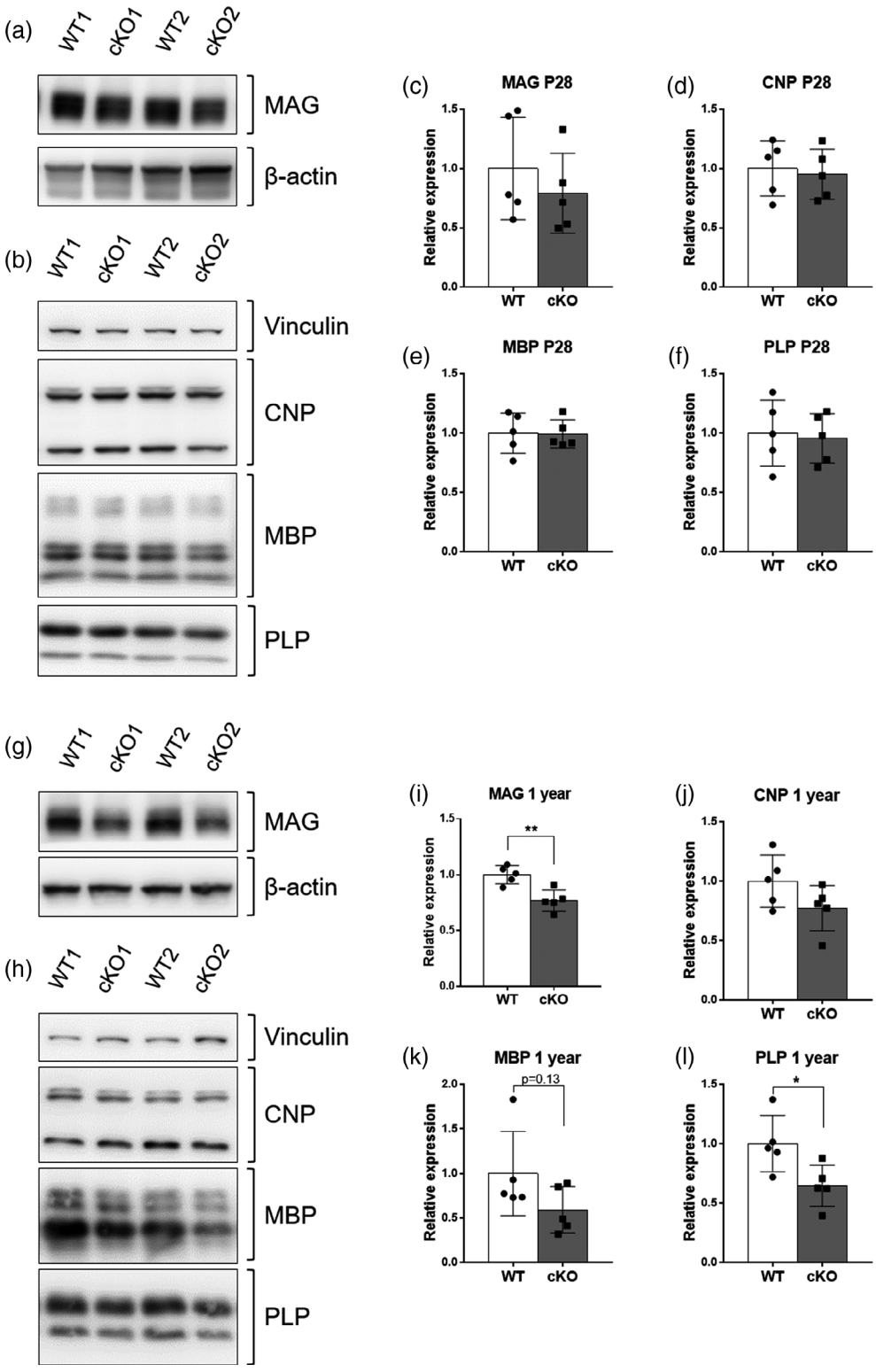

FIGURE 4 Cyclin-dependent kinase 7 (Cdk7) invalidation leads to a reduced amount of myelin proteins in aged mice. (a, g) Representative images of MAG western blot with protein extracts from lumbar spinal cord of WT and cKO mice at (a) P28 and (g) 1 year. β-actin serves as a loading control. (b, h) Representative images of CNP, MBP and PLP western blot with protein extracts from lumbar spinal cord of WT and cKO mice at (b) P28 and (h) 1 year. Vinculin serves as a loading control. (c, i) Quantification of MAG protein expression relative to β-actin at (c) P28 and (i) 1 year. (d–f and j–l) Quantification of (d and j) CNP, (e and k) MBP and (f and l) PLP protein expression relative to vinculin at (d–f) P28 and (j–l) 1 year ($n = 5$ for all groups; *: $p < .05$; **: $p < .01$, two-tailed t test).

an O4 immunostaining (Figure 6a) and quantified the morphological changes induced by cAMP and/or YKL-5-124 treatment thanks to a Sholl analysis. This analysis compares cell morphology complexity by counting the number of intersections made with concentric circles of increasing diameter relative to the distance from the cell center (Figure 6b). As expected, cAMP treatment induced typical changes of the morphology, with the development of a more complex cell branching. Quantification revealed that this more complex morphology was associated with a statistically higher number of intersections. However, the cAMP-induced increase of morphological complexity was significantly reduced when cells were also treated with YKL-5-124 (Figure 6c).

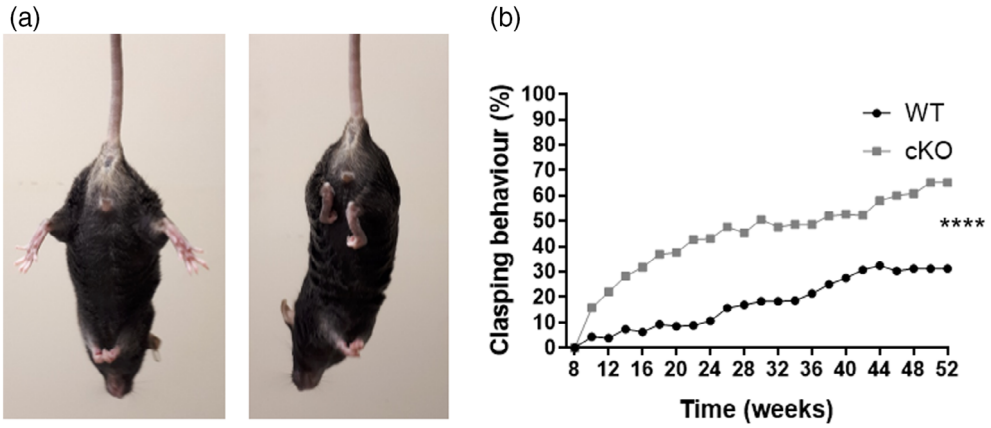

FIGURE 5 Cyclin-dependent kinase 7 (Cdk7) invalidation is associated with hindlimb clasping behavior. (a) Representative pictures of mice during the hindlimb clasping test. Left: no clasping; right: clasping behavior. (b) Quantification of the percentage of mice exhibiting a hindlimb clasping behavior, in WT and cKO mice from 8 to 52-weeks-old ($n = 20–30$ for both groups, ****: $p < .0001$, Two-way ANOVA).

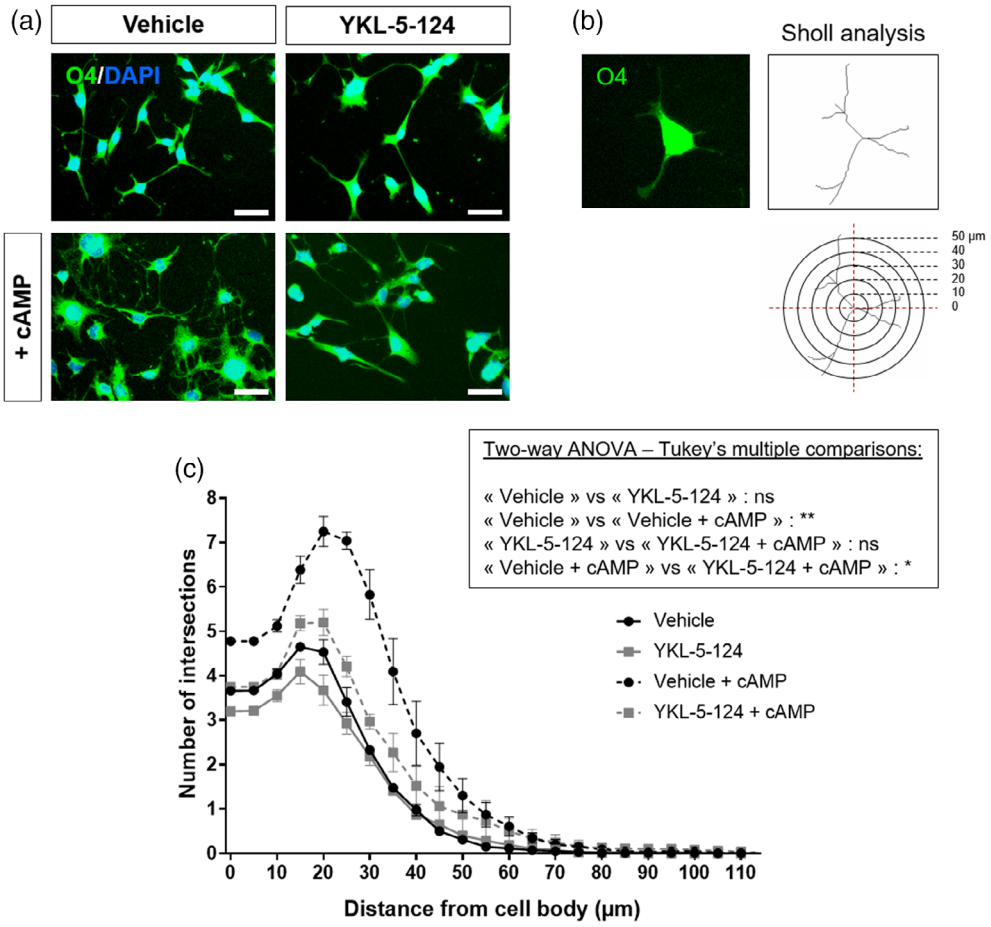

FIGURE 6 YKL-5-124 treatment alters Oli-neu cells cAMP-induced morphological changes. (a) Representative images of O4 immunostaining in Oli-neu cells in control condition (Vehicle) or treated with YKL-5-124 (250 nM) and/or cAMP (1 mM) for 3 days. Nuclei are stained with DAPI. Scalebar = 50 µm. (b) Schematic representation of Sholl analysis. O4-labeled isolated cells were selected and cell projections were manually traced. Concentric circles with an increasing diameter were placed from the center of the cell, and the number of intersections with each circle was counted. (c) Sholl analysis of Oli-neu cells in control condition (Vehicle), treated with YKL-5-124 only (YKL-5-124), cAMP only (Vehicle + cAMP) or YKL-5-124 and cAMP (YKL-5-124 + cAMP) for3 days (n.s.: non significant; *: $p < .05$; **: $p < .01$, Two-way ANOVA—Tukey's multiple comparisons).

Since Cdk7 is known to be involved in the regulation of gene transcription, we then used the same model to measure the expression level of mRNAs coding for proteins that are particularly important in the oligodendroglial lineage.

Cdk7 mRNA expression was neither modified by cAMP nor by YKL-5-124 treatments (Figure 7a). As expected, mRNA levels of myelin genes such as *Mag*, *Mog* and *Plp*, of the post-mitotic oligodendrocyte marker *Cnp*, and of the major positive transcriptional regulator of CNS myelination *Myrf*, were all strongly increased when cells were treated with cAMP. Interestingly, the increased expression of these genes was hampered by YKL-5-124 treatment (Figure 7b–f).

Altogether, our in vitro results confirm that the myelination process is somehow impaired in absence of Cdk7 activity, possibly through the regulation of transcriptional programs involved in myelin gene expression.

5 | DISCUSSION

Myelin is essential to allow a fast conduction of action potentials along the axons and to provide them metabolic support. During development, CNS myelin is generated through the differentiation of OPCs

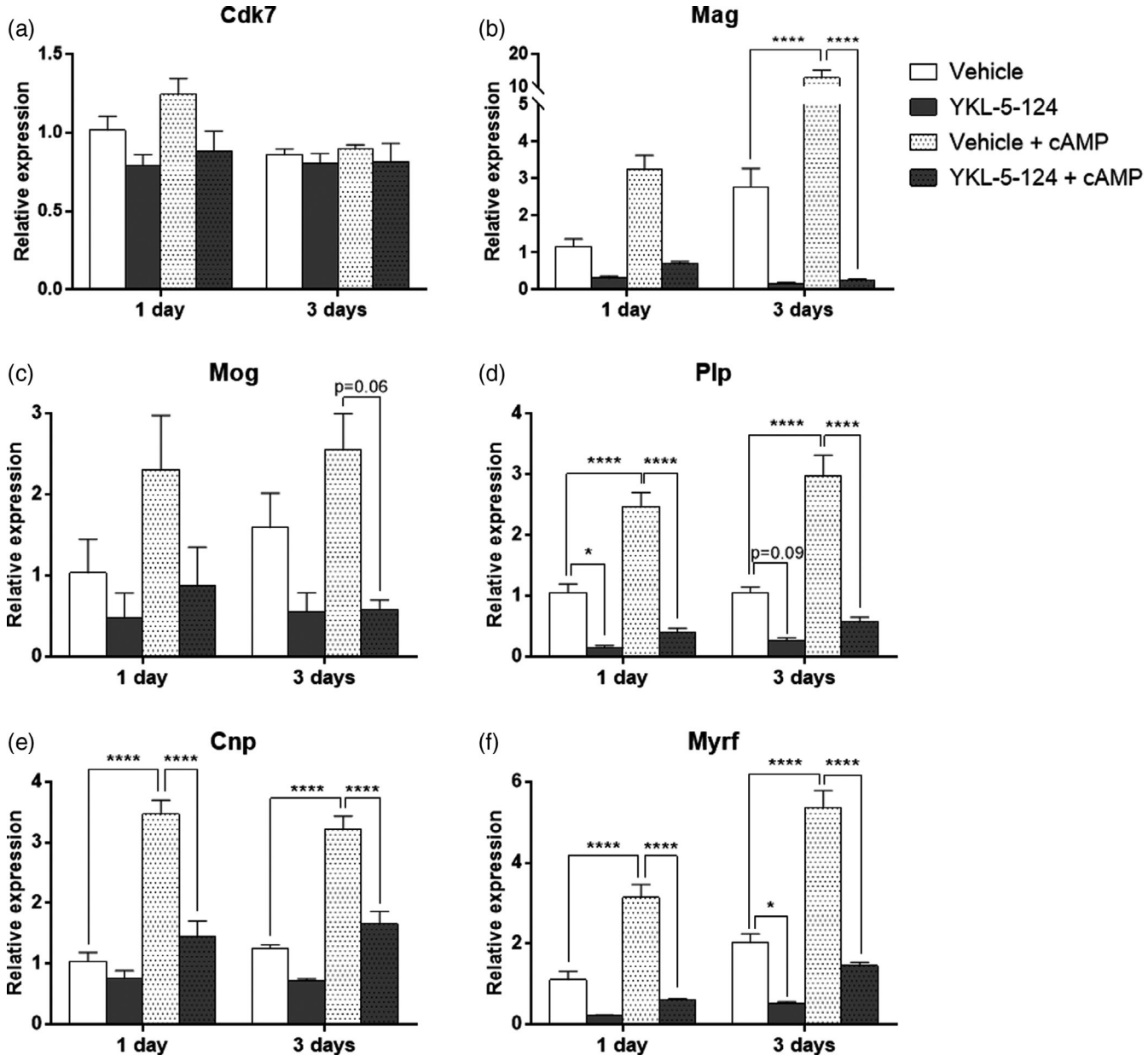

FIGURE 7 YKL-5-124 treatment decreases mRNA expression of myelin-specific genes. (a–f) Quantification of mRNA relative expression by RT-qPCR in Oli-neu cells in control condition (Vehicle), treated with YKL-5-124 (250 nM) only (YKL-5-124), cAMP (1 mM) only (Vehicle + cAMP) or YKL-5-124 and cAMP (YKL-5-124 + cAMP) for one or 3 days. mRNA expression was quantified for (a) *Cdk7*, (b) *Mag*, (c) *Mog*, (d) *Plp*, (e) *Cnp* and (f) *Myrf*. (*: $p < .05$; ****: $p < .0001$, Two-way ANOVA—Tukey's multiple comparisons).

into myelin-forming oligodendrocytes. However, OPCs retain the ability to generate new oligodendrocytes in the adult CNS which allows to regenerate myelin during normal aging or in pathological conditions. Even if some pathways are conserved, the mechanisms regulating developmental myelination or myelin maintenance in adulthood are not exactly the same, and not yet fully described (Bergles & Richardson, 2015; Stadelmann et al., 2019). A better understanding of these molecular mechanisms is especially interesting in the context of CNS demyelinating diseases, as most of them occur during adulthood when the myelin structure has already been established. In our study, we hypothesized that Cdk7 might be one of those regulating factors. We verified this hypothesis by generating a conditional knock-out model in which Cdk7 is invalidated in post-mitotic oligodendrocytes, and investigated the underlying mechanisms using an in vitro oligodendroglial model.

5.1 | Cdk7 is mostly dispensable for normal developmental myelination but its invalidation progressively leads to myelin defects

Cdk7 is involved in cell cycle progression and in transcription regulation. In order to investigate its role in a strictly transcriptional context—independently of its role in cell cycle—we generated a

conditional knock-out model in which Cdk7 is invalidated in post-mitotic oligodendrocytes, and we analyzed if this invalidation affected myelination during postnatal development and in adult mice. At P28—a stage corresponding to the end of the developmental myelination in the CNS—we observed a similar number of myelinated axons in the spinal cord of WT and cKO animals, even though the mean axonal diameter and the proportion of large caliber myelinated axons were reduced in cKO mice. The myelin sheath thickness and myelin protein contents were comparable between WT and cKO animals. These results indicate that Cdk7 is mostly dispensable for normal developmental myelination.

However, stronger myelin defects began to appear in the spinal cord of adult cKO mice. Indeed, in adult mice aged of 8–10 weeks, we could already detect some abnormalities, and these were even more pronounced in 1-year-old mice. These defects included an increased number of small caliber myelinated axons associated with a reduction of the mean axonal diameter and a reduced proportion of large caliber myelinated axons, an increased number of post-mitotic oligodendrocytes, a thinner myelin sheath in large caliber axons, and a decreased amount of myelin proteins.

A similar phenotype has been observed in a model of neonatal hypoxia, in which an initial loss of oligodendrocytes due to hypoxia was later on compensated by an increased number of oligodendrocytes, but not accompanied by a normal axonal myelination (Jablonska et al., 2012). Signs of imperfect myelin wrapping around axons and an increased number of small caliber myelinated axons associated with a reduced mean axonal diameter has also been observed in another study using the hypoxia model (Watzlawik et al., 2015). In our case, we hypothesize that the increased number of small diameter myelinated axons correlates to the higher number of post-mitotic oligodendrocytes.

Interestingly, a hindlimb clasping behavior started to appear in mice as soon as 10-weeks-old, and the overall percentage of mice exhibiting this behavior was significantly higher in cKO mice. Hindlimb clasping is a neurologic sign often found in transgenic or experimental mouse models of neurodegenerative diseases. It is associated with lesions or abnormalities in different areas of the spinal cord or the brain, and commonly due either to myelin defects or to axonal degeneration (Adebola et al., 2015; Cahill et al., 2019; De Pace et al., 2018; Scherz et al., 2018). In our study, it is unlikely that the behavior is due to axonal degeneration, as we could not observe signs of increased axonal damage or of axonal shrinkage. We thus believe that the myelin defects observed in the cKO animals were sufficient to induce the hindlimb clasping phenotype. It would be interesting to perform further behavioral analysis to fully understand the functional consequences of those myelin defects.

In summary, our results indicate that Cdk7 invalidation in oligodendrocytes allows normal myelination in postnatal development but progressively leads to myelin defects in aged mice, and that these defects are responsible for the development of an abnormal behavior. Interestingly, a similar phenotype was observed in the PNS when Mat1—one of the three components of the CAK complex, along with Cdk7 and Cyclin H—was invalidated in Schwann cells. Indeed, in those mice, a normal myelination of the sciatic nerve was followed by a progressive demyelination starting after 3 months of age (Korsisaari et al., 2002). As the other subunits of the CAK complex are degraded when either Mat1 or Cdk7 are absent (Ganuza et al., 2012; Korsisaari et al., 2002), we can assume that Cdk7 invalidation in Schwann cells would have the same consequences as with Mat1 invalidation.

5.2 | Cdk7 inhibition alters the expression of myelination-associated genes

Cdk7 is known to regulate gene transcription through the phosphorylation of RNA Pol II and of some nuclear receptors (Fisher, 2005). Although the importance of Cdk7-mediated gene expression has been extensively studied in the context of cancer (Chipumuro et al., 2014; Christensen et al., 2014; Kwiatkowski et al., 2014; Wang et al., 2015), its role in the normal functioning of the CNS remains poorly understood. Using an in vitro oligodendroglial model, we showed that pharmacological inhibition of Cdk7 prevents the acquisition of a more complex morphology characteristic of early myelination and reduces the expression of important myelination-associated genes.

We observed that YKL-5-124 treatment limited the acquisition of a more complex cell branching. These morphological changes are necessary in early myelination to allow target recognition and axonal wrapping, and their reduction indicate that the myelination process is somehow impaired when Cdk7 is inhibited.

In addition, when the myelination process was initiated, we observed an increased expression of *Mag*, *Mog*, *Plp*, *Cnp* and *Myrf* genes, which was strongly reduced by YKL-5-124 treatment. Those genes code for four myelin proteins—MAG, MOG, PLP and CNP—and for the transcription factor Myelin regulatory factor (MYRF), respectively. MYRF is a major transcription factor in oligodendrocytes and is essential for the initiation and maintenance of their myelination program (Emery et al., 2009). The downregulated expression of myelination-associated genes we observed could thus be the consequence of a reduction in MYRF. Future experiments will decipher whether Cdk7 modulates all these genes independently or acts specifically through MYRF.

Interestingly, it was shown that MYRF is not necessary for the generation of OPCs and their differentiation into pre-myelinating oligodendrocytes, but that it is required for the generation of mature oligodendrocytes, their expression of myelin genes and myelin formation during development, and also for the maintenance of myelin and mature oligodendrocyte identity in adulthood (Emery et al., 2009; Koenning et al., 2012). An impaired expression of MYRF could thus possibly explain the progressively appearing myelin defects we observed in our cKO mouse model.

5.3 | Therapeutic perspectives

It is well known that human demyelinating diseases—such as MS in the CNS—arise mainly in adulthood, after the myelin structure is fully formed. A better understanding of the molecular mechanisms that

maintain myelin integrity and preserve axonal function in adulthood is thus crucial. Our study allowed us to uncover a new role of Cdk7 in CNS myelination. Even though it is dispensable for normal myelination during the CNS development, its absence progressively leads to myelin defects in adulthood. The precise mechanisms involved in this Cdk7-dependent role are still unknown and the kinase substrates have yet to be defined. Their description might be useful in order to develop new protective or therapeutic strategies in demyelinating pathologies.

ACKNOWLEDGMENTS

This work was supported by Grants from the Belgian Fund for Scientific Research (F.R.S.—FNRS), the Léon Fredericq Foundation from the University of Liege, the Charcot Foundation from Belgium, and the Faculty of Medicine of the University of Liege. We are also grateful to the GIGA-Cell Imaging platform from the GIGA-Research center of the University of Liege. Nathalie Schumacher is FRIA grantee of the Belgian Fund for Scientific Research (F.R.S. -FNRS). We thank Dr J. Trotter (University of Mainz, Germany) for Oli-neu cell line, Drs D. Santamaria and M. Barbacid (Centro Nacional de Investigaciones Oncológicas, Madrid, Spain) for Cdk7^{lox} mice and Dr. N. Gray (Harvard Medical School and the Dana Farber Cancer Institute, Boston, MA, USA) for covalent Cdk7 inhibitor. The authors also acknowledge Animascience for table of contents image illustration, for which figure rights have been transferred to the authors.

DATA AVAILABILITY STATEMENT

The data that support the findings of this study are available from the corresponding author upon reasonable request.

ORCID

Valérie Dion https://orcid.org/0000-0002-3489-1062
Pierre Tocquin https://orcid.org/0000-0002-1302-6504
Brigitte Malgrange https://orcid.org/0000-0002-8957-2528
Renaud Vandenbosch https://orcid.org/0000-0003-4887-9870
Rachelle Franzen https://orcid.org/0000-0001-7336-791X

REFERENCES

Adebola, A. A., Di Castri, T., He, C-Z., Salvatierra, L. A., Zhao, J., Brown, K., Worman, H. J., & Liem, R. K. H. (2015). Neurofilament light polypeptide gene N98S mutation in mice leads to neurofilament network abnormalities and a Charcot–Marie-Tooth Type 2E phenotype. *Human Molecular Genetics*, *24*(8), 2163–2174. https://doi.org/10.1093/hmg/ddu736

Bauer, N. G., Richter-Landsberg, C., & Ffrench-Constant, C. (2009). Role of the oligodendroglial cytoskeleton in differentiation and myelination. *Glia*, *57*(16), 1691–1705. https://doi.org/10.1002/glia.20885

Bergles, D. E., & Richardson, W. D. (2015). Oligodendrocyte development and plasticity. *Cold Spring Harbor Perspectives in Biology*, *8*(2), a020453. https://doi.org/10.1101/cshperspect.a020453

Cahill, L. S., Zhang, M. A., Ramaglia, V., Whetstone, H., Sabbagh, M. P., Yi, T. J., Woo, L., Przybycien, T. S., Moshkova, M., Zhao, F. L., Rojas, O. L., Gomes, J., Kuerten, S., Gommerman, J.L., Sled, J. G., & Dunn, S. E. (2019). Aged hind-limb clasping experimental autoimmune encephalomyelitis models aspects of the neurodegenerative process seen in multiple sclerosis. *Proceedings of the National Academy of Sciences of the United States of America*, *116*(45), 22710–22720. https://doi.org/10.1073/pnas.1915141116

Chen, D., Riedl, T., Washbrook, E., Pace, P. E., Coombes, R. C., Egly, J. M., & Ali, S. (2000). Activation of estrogen receptor alpha by S118 phosphorylation involves a ligand-dependent interaction with TFIIH and participation of CDK7. *Molecular Cell*, *6*(1), 127–137.

Chipumuro, E., Marco, E., Christensen, C. L., Kwiatkowski, N., Zhang, T., Hatheway, C. M., Abraham, B. J., Sharma, B., Yeung, C., Altabef, A., Perez-Atayde, A., Wong, K-K., Yuan, G-C., Gray, N. S., Young, R. A., & George, R. E. (2014). CDK7 inhibition suppresses super-enhancer-linked oncogenic transcription in MYCN-driven cancer. *Cell*, *159*(5), 1126–1139. https://doi.org/10.1016/j.cell.2014.10.024

Christensen, C. L., Kwiatkowski, N., Abraham, B. J., Carretero, J., Al-Shahrour, F., Zhang, T., Chipmuro, E., Herter-Sprie, G. S., Akbay, E. A., Altabef, A., Zhang, J., Shimamura, T., Capelletti, M., Reibel, J. B., Cavanaugh, J. D., Gao, P., Liu, Y., Michaelsen, S. R., Poulsen, H. S., … Wong, K. K. (2014). Targeting transcriptional addictions in small cell lung cancer with a covalent CDK7 inhibitor. *Cancer Cell*, *26*(6), 909–922. https://doi.org/10.1016/j.ccell.2014.10.019

Compe, E., Drané, P., Laurent, C., Diderich, K., Braun, C., Hoeijmakers, J. H., & Egly, J. M. (2005). Dysregulation of the peroxisome proliferator-activated receptor target genes by XPD mutations. *Molecular and Cellular Biology*, *25*(14), 6065–6076. https://doi.org/10.1128/mcb.25.14.6065-6076.2005

Compe, E., & Egly, J. M. (2012). TFIIH: When transcription met DNA repair. *Nature Reviews. Molecular Cell Biology*, *13*(6), 343–354. https://doi.org/10.1038/nrm3350

Compe, E., Malerba, M., Soler, L., Marescaux, J., Borrelli, E., & Egly, J. M. (2007). Neurological defects in trichothiodystrophy reveal a coactivator function of TFIIH. *Nature Neuroscience*, *10*(11), 1414–1422. https://doi.org/10.1038/nn1990

Compston, A., & Coles, A. (2008). Multiple sclerosis. *Lancet*, *372*(9648), 1502–1517. https://doi.org/10.1016/s0140-6736(08)61620-7

Cunniffe, N., & Coles, A. (2019). Promoting remyelination in multiple sclerosis. *Journal of Neurology*, *268*, 30–44. https://doi.org/10.1007/s00415-019-09421-x

De Pace, R., Skirzewski, M., Damme, M., Mattera, R., Mercurio, J., Foster, A. M., Cuitino, L., Jarnik, M., Hoffmann, V., Morris, H. D., Han, T-U., Mancini, G. M. S., Buonanno, A., & Bonifacino, J. S. (2018). Altered distribution of ATG9A and accumulation of axonal aggregates in neurons from a mouse model of AP-4 deficiency syndrome. *PLoS Genetics*, *14*(4), e1007363. https://doi.org/10.1371/journal.pgen.1007363

Emery, B. (2010). Regulation of oligodendrocyte differentiation and myelination. *Science*, *330*(6005), 779–782. https://doi.org/10.1126/science.1190927

Emery, B., Agalliu, D., Cahoy, J. D., Watkins, T. A., Dugas, J. C., Mulinyawe, S. B., Ibrahim, A., Ligon, K. L., Rowitch, D. H., & Barres, B. A. (2009). Myelin gene regulatory factor is a critical transcriptional regulator required for CNS myelination. *Cell*, *138*(1), 172–185. https://doi.org/10.1016/j.cell.2009.04.031

Emery, B., & Lu, Q. R. (2015). Transcriptional and epigenetic regulation of oligodendrocyte development and myelination in the central nervous system. *Cold Spring Harbor Perspectives in Biology*, *7*(9), a020461. https://doi.org/10.1101/cshperspect.a020461

Fisher, R. P. (2005). Secrets of a double agent: CDK7 in cell-cycle control and transcription. *Journal of Cell Science*, *118*(Pt 22), 5171–5180. https://doi.org/10.1242/jcs.02718

Ganuza, M., Saiz-Ladera, C., Canamero, M., Gomez, G., Schneider, R., Blasco, M. A., Pisano, D., Paramio, J. M., Santamaria, D., & Barbacid, M. (2012). Genetic inactivation of Cdk7 leads to cell cycle arrest and induces premature aging due to adult stem cell exhaustion. *The EMBO Journal*, *31*(11), 2498–2510. https://doi.org/10.1038/emboj.2012.94

He, G., Yang, X., Wang, G., Qi, J., Mao, R., Wu, Z., & Zhou, Z. (2017). Cdk7 is required for activity-dependent neuronal gene expression, long-

lasting synaptic plasticity and long-term memory. *Frontiers in Molecular Neuroscience*, *10*, 365. https://doi.org/10.3389/fnmol.2017.00365

Jablonska, B., Scafidi, J., Aguirre, A., Vaccarino, F., Nguyen, V., Borok, E., Horvath, T.L., Rowitch, D.H., & Gallo, V. (2012). Oligodendrocyte regeneration after neonatal hypoxia requires FoxO1-mediated p27Kip1 expression. *The Journal of Neuroscience*, *32*(42), 14775–14793. https://doi.org/10.1523/jneurosci.2060-12.2012

Jung, M., Krämer, E., Grzenkowski, M., Tang, K., Blakemore, W., Aguzzi, A., Khazaie, K., Chlichlia, K., von Blankenfeld, G., & Kettenmann, H. (1995). Lines of murine oligodendroglial precursor cells immortalized by an activated neu tyrosine kinase show distinct degrees of interaction with axons in vitro and in vivo. *The European Journal of Neuroscience*, *7*(6), 1245–1265. https://doi.org/10.1111/j.1460-9568.1995.tb01115.x

Koenning, M., Jackson, S., Hay, C. M., Faux, C., Kilpatrick, T. J., Willingham, M., & Emery, B. (2012). Myelin gene regulatory factor is required for maintenance of myelin and mature oligodendrocyte identity in the adult CNS. *The Journal of Neuroscience*, *32*(36), 12528–12542. https://doi.org/10.1523/jneurosci.1069-12.2012

Korsisaari, N., Rossi, D. J., Paetau, A., Charnay, P., Henkemeyer, M., & Makela, T. P. (2002). Conditional ablation of the Mat1 subunit of TFIIH in Schwann cells provides evidence that Mat1 is not required for general transcription. *Journal of Cell Science*, *115*(Pt 22), 4275–4284. https://doi.org/10.1242/jcs.00121

Kwiatkowski, N., Zhang, T., Rahl, P. B., Abraham, B. J., Reddy, J., Ficarro, S. B., Dastur, A., Amzallag, A., Ramaswamy, S., Tesar, B., Jenkins, C. E., Hannett, N. M., McMillin, M. C., Sanda, T., Sim, T., Kim, N. D., Look, T., Mitsiades, C., Weng, A. P., … Gray, N. S. (2014). Targeting transcription regulation in cancer with a covalent CDK7 inhibitor. *Nature*, *511*(7511), 616–620. https://doi.org/10.1038/nature13393

Lalonde, R., & Strazielle, C. (2011). Brain regions and genes affecting limb-clasping responses. *Brain Research Reviews*, *67*(1–2), 252–259. https://doi.org/10.1016/j.brainresrev.2011.02.005

Lappe-Siefke, C., Goebbels, S., Gravel, M., Nicksch, E., Lee, J., Braun, P. E., & Griffiths, I. R., & Nave, K-A. (2003). Disruption of Cnp1 uncouples oligodendroglial functions in axonal support and myelination. *Nature Genetics*, *33*(3), 366–374. https://doi.org/10.1038/ng1095

Li, B. B., Wang, B., Zhu, C. M., Tang, D., Pang, J., Zhao, J., Sun, C-H., Qiu, M-J., & Qian, Z-R. (2019). Cyclin-dependent kinase 7 inhibitor THZ1 in cancer therapy. *Chronic Diseases and Translational Medicine*, *5*(3), 155–169. https://doi.org/10.1016/j.cdtm.2019.08.006

Malumbres, M., & Barbacid, M. (2005). Mammalian cyclin-dependent kinases. *Trends in Biochemical Sciences*, *30*(11), 630–641. https://doi.org/10.1016/j.tibs.2005.09.005

Olson, C. M., Liang, Y., Leggett, A., Park, W. D., Li, L., Mills, C. E., Elsarrag, S. Z., Ficarro, S. B., Zhang, T., Düster, R., Geyer, M., Sim, T., Marto, J. A., Sorger, P. K., Westover, K. D., Lin, C. Y., Kwiatkowski, N., & Gray, N. S. (2019). Development of a selective CDK7 covalent inhibitor reveals predominant cell-cycle phenotype. *Cell Chemical Biology*, *26*(6), 792–803. e710. https://doi.org/10.1016/j.chembiol.2019.02.012

Rochette-Egly, C., Adam, S., Rossignol, M., Egly, J. M., & Chambon, P. (1997). Stimulation of RAR alpha activation function AF-1 through binding to the general transcription factor TFIIH and phosphorylation by CDK7. *Cell*, *90*(1), 97–107. https://doi.org/10.1016/s0092-8674(00)80317-7

Scherz, B., Rabl, R., Flunkert, S., Rohler, S., Neddens, J., Taub, N., Temmel, M., Panzenboeck, U., Niederkofler, V., Zimmermann, R., & Hutter-Paier, B. (2018). mTh1 driven expression of hTDP-43 results in typical ALS/FTLD neuropathological symptoms. *PLoS ONE*, *13*(5), e0197674. https://doi.org/10.1371/journal.pone.0197674

Simons, M., & Nave, K. A. (2015). Oligodendrocytes: Myelination and axonal support. *Cold Spring Harbor Perspectives in Biology*, *8*(1), a020479. https://doi.org/10.1101/cshperspect.a020479

Stadelmann, C., Timmler, S., Barrantes-Freer, A., & Simons, M. (2019). Myelin in the central nervous system: Structure, function, and pathology. *Physiological Reviews*, *99*(3), 1381–1431. https://doi.org/10.1152/physrev.00031.2018

Wang, M., Wang, T., Zhang, X., Wu, X., & Jiang, S. (2020). Cyclin-dependent kinase 7 inhibitors in cancer therapy. *Future Medicinal Chemistry*, *12*(9), 813–833. https://doi.org/10.4155/fmc-2019-0334

Wang, Y., Zhang, T., Kwiatkowski, N., Abraham, B. J., Lee, T. I., Xie, S., Yuzugullu, H., Von, T., Li, H., Lin, Z., Stover, D. G., Lim, E., Wang, Z. C., Iglehart, J. D., Young, R. A., Gray, N. S., & Zhao, J. J. (2015). CDK7-dependent transcriptional addiction in triple-negative breast cancer. *Cell*, *163*(1), 174–186. https://doi.org/10.1016/j.cell.2015.08.063

Watzlawik, J. O., Kahoud, R. J., O'Toole, R. J., White, K. A., Ogden, A. R., Painter, M. M., Wootla, B., Papke, L. M., Denic, A., Weimer, J. M., Carey, W. A., & Rodriguez, M. (2015). Abbreviated exposure to hypoxia is sufficient to induce CNS dysmyelination, modulate spinal motor neuron composition, and impair motor development in neonatal mice. *PLoS ONE*, *10*(5), e0128007. https://doi.org/10.1371/journal.pone.0128007

SUPPORTING INFORMATION

Additional supporting information may be found in the online version of the article at the publisher's website.

How to cite this article: Dion, V., Schumacher, N., Masar, N., Pieltain, A., Tocquin, P., Lesoinne, P., Malgrange, B., Vandenbosch, R., & Franzen, R. (2022). Cyclin-dependent kinase 7 contributes to myelin maintenance in the adult central nervous system and promotes myelin gene expression. *Glia*, 1–14. https://doi.org/10.1002/glia.24186